Journal of Catalysis **194,** 330–342 (2000)
doi:10.1006/jcat.2000.2926, available online at http://www.idealibrary.com on IDEAL®

Structure, Distribution, and Properties of Co Ions in Ferrierite Revealed by FTIR, UV–Vis, and EXAFS

Zdeněk Sobalík,* Jiří Dědeček,* Dalibor Kaucký,* Blanka Wichterlová,*,[1]
Lucie Drozdová,† and Roel Prins†

*J. Heyrovský Institute of Physical Chemistry, Academy of Sciences of the Czech Republic, Dolejškova 3, CZ-182 23 Prague 8, Czech Republic; and †Laboratory for Technical Chemistry, Swiss Federal Institute of Technology, ETH-Zentrum Universitätstrasse 6, Zürich, CH-8092 Switzerland
E-mail: wichterl@jh-inst.cas.cz.

Received February 24, 2000; revised May 17, 2000; accepted May 19, 2000

Ion-exchanged Co ions and nitrosyl complexes in CoH– and CoNaK–ferrierites with a Co loading up to Co/Al = 0.4 were investigated by diffuse reflectance UV–Vis–NIR, FTIR in the region of the skeletal and NO vibrations, and EXAFS measurements. Co(II) ion coordination, cation-induced perturbations of the framework T–O bonds of the hosted cationic sites, and Co–O distances of three typical ion-exchanged α-, β-, and γ-type Co ions in ferrierite are described. The α-type Co ions, coordinated to the rectangle of framework oxygens in the wall of the main ten-member ring channel, exhibit an open coordination sphere, weak bonding to the framework oxygens, and a high tendency to form dinitrosyl complexes upon NO adsorption. The β-type Co ions, the most populated ones in the whole concentration range, are coordinated to four framework oxygens of the deformed six-member ring of the ferrierite cavity at a distance of 1.99 Å. They exhibit medium-strength bonding to framework oxygens and, compared to the α-type Co ions, a substantially suppressed ability to bind dinitrosyls. The γ-type Co ions provide the highest perturbation of the hosted framework T–O bonds and thus the strongest bonding to framework oxygens attributed to the "boat-shaped" site of ferrierite. The tendency of the Co ions to relocalize under severe thermal/hydrothermal calcination of Co–ferrierite increased in the sequence $\gamma < \beta \ll \alpha$, in agreement with the strength of bonding of the Co ions to framework oxygens at cationic sites.

Key Words: **Co ions in zeolites; ferrierite; Co ion Vis spectra; IR skeletal vibrations; EXAFS; Co–NO complexes.**

INTRODUCTION

Transition-metal ions, particularly Co and Cu, planted in pentasil ring zeolites with MOR, MFI, FER, and BEA topologies with a low concentration of aluminium in their framework (Si/Al molar ratios ranging from 8 to 20) exhibit exceptional activity/selectivity in the decomposition of NO (Cu) (1–3) and in the selective catalytic reduction of NO_x with low paraffins in an oxidizing atmosphere (Cu, Co, Fe) (4–6) including methane (Co, Ga) (7–10). The high activity/selectivity of these materials in such specific and demanding catalytic reactions have induced a high interest in the elucidation of the structure of the metal ions in these zeolites and its relationship to their catalytic properties (3, 11). Determining the environment of the exchanged metal ions and distinguishing it from cations in metal oxide species possibly present in some zeolites may provide basic information needed for the elucidation of the exceptional catalytic properties of the metal–zeolites.

Generally, the cationic sites of transition-metal ions in dehydrated pentasil ring zeolites of MOR, MFI, FER, and BEA topologies have not been determined, and only the siting of non-transition-metal ions in dehydrated mordenite was established by XRD studies (12). However, a standard XRD analysis of the location of transition-metal ions in these zeolites could not be applied because of the low concentration of the metal ions, the large unit cell, and the expected distribution of the metal ions among several cationic sites. Only synchrotron powered X-ray diffraction resolved the cationic sites for Cu(II) in mordenite (13). EXAFS studies carried out with Cu–ZSM-5 (13–15), Co–Beta (16), and Co–ZSM-5 (17) were not able to establish the siting of the metal ions.

This low level of information on the structure of the exchanged transition-metal ions stimulated our studies on Cu(II) and Cu(I) (18–21) and Co(II) (22–24) siting in pentasil ring zeolites employing a combination of several spectroscopic techniques such as UV–Vis–NIR, FTIR of probe molecules, ESR, and emission in Vis spectra. Based on the similarities in both the characteristic spectral components of the Co(II) ions and the known local framework geometries in mordenite, ferrierite, and ZSM-5, three characteristic Co(II) ion sites were determined in each of these zeolites and denoted as α, β, and γ sites (22–24). The α-type Co ions were suggested to be located in the main channels of mordenite and ferrierite and the straight channel of the ZSM-5 structure, coordinated to framework oxygens of the six-member rings composed of five-member rings. The β-type

[1] To whom correspondence should be addressed.

0021-9517/00 $35.00

Co ions are located in the twisted eight-member rings of the mordenite cavity, in the deformed six-member rings of the ferrierite cavity, and at the deformed six-member ring at the intersection of the straight and sinusoidal channels of the ZSM-5 structure. The Co ions in the γ site are in the so-called "boat-shaped" site of mordenite (see Ref. (12)) and analogous framework local structures found in ferrierite and ZSM-5 (cf. Refs. (23) and (24), respectively).

It has also been shown that the coordination of transition-metal ions to framework oxygens is reflected in the local changes in vibrations of the framework T–O bonds (25–27). The background of this effect was described by van Santen and Vogel for aluminium-rich zeolites such as faujasite and zeolite A (28). For high-silica zeolites, the unperturbed antisymmetric vibration of the framework T–O bonds at ca. 1100 cm^{-1} is shifted to lower frequency, into the transmission window between 900 and 950 cm^{-1}, forming the B_M band, denoted as the "deformation shift." We have shown that the position of the B_M band, reflecting the extent of perturbation of the framework T–O bonds, depends on the nature of the cation (27) and reflects the degree of ionicity and covalency of cation bonding to framework oxygens (29). This spectral mode of skeletal vibrations was also used to detect the valency of copper (30) and the presence of Co(II) ions in ZSM-5 (31) and ferrierite (27).

As a result of coordination of extraframework ligands to the cation, the characteristic B_M band is shifted to higher frequencies ("relaxation shift"). This general effect was demonstrated for the complexes of Co(II) ions with NH_3 and H_2O (27, 32), NO, CO, and NO_2 (32), and amines and nitriles (33) in zeolites.

In the present paper an attempt is made to describe the coordination and behaviour of the exchanged Co ions in ferrierite using complementary spectroscopic techniques reflecting Co ion coordination, perturbation of hosted framework bonds, and Co–O distances. It is shown that the Co ions coordinated at cationic sites exhibit characteristic Co–O bond lengths and induce a characteristic perturbation of the adjacent framework T–O bonds. This is revealed by simultaneous monitoring of the Co(II) Vis spectra, IR vibrations of the T–O framework bonds, and EXAFS spectra. Quantitative analysis of the spectroscopic results for Co–ferrierite under thermal/hydrothermal treatments and adsorption of NO provides a description of the polyoxoanionic–cobalt–(extraframework ligand) complexes in the zeolite. Thus, a detailed insight into the structure, strength of bonding, distribution/redistribution, and complexation of the Co ions in ferrierite is given. The presence of cobalt oxide species, besides the true exchanged Co ions, as reflected in the above spectra is discussed as well.

In the subsequent paper (34) catalytic activity of individual α-, β-, and γ-type Co ions exchanged in FER, MOR, and MFI zeolite structures is reported and the different activity of the Co ions planted in various zeolite matrices is analyzed.

EXPERIMENTAL

Materials

Parent NaK– and NH_4–ferrierite. XRD analysis and IR spectra of skeletal vibrations evidenced that NaK–FER, Si/Al 8.4 (TOSOH Co., Japan) was a pure crystalline material. NH_4–FER was prepared from NaK–FER by four times repeated ion exchange at room temperature (RT) using 1.0 M NH_4NO_3 (10 ml/1 g of zeolite) to reach complete NH_4^+ exchange. Then the zeolites were thoroughly washed with distilled water and dried in air.

Co–ferrierite preparation. $CoNH_4$–FER samples with Co concentrations of 0.40–3.62 wt% were prepared by ion exchange of NH_4–FER with 0.05–0.1 M Co acetate at 70°C, and CoNaK–FER samples with a Co concentration of 0.12–2.60 wt% were prepared by ion exchange of NaK–FER with 0.001–0.05 M $Co(NO_3)_2$ at RT and 70°C. A detailed description of the preparation of Co–ferrierites is given in Ref. (23). Table 1 provides the chemical composition of the Co–zeolites. A molar ratio of Co/Al = 0.5 corresponds to the stoichiometric exchange degree, as the Co ions were in the divalent state after all treatments of the Co–ferrierites.

Co–ferrierite treatments. Prior to the UV–Vis–NIR, FTIR, and EXAFS spectra measurements the Co–FERs were pretreated at elevated temperatures. Two types of treatments were applied: (i) a "standard *in situ*" heat treatment at 480°C for 3 h (temperature increase of 5°C/min) under a dynamic vacuum of 10^{-2} Pa and (ii) a heat treatment at 550°C for 12 h in air followed by zeolite hydration at RT and subsequent dehydration of the sample by the standard *in situ* treatment given above. After the standard *in situ* treatment, the samples were cooled to RT in vacuum and the spectra were recorded at RT. Samples prepared for UV–Vis–NIR measurements were in the form of small grains (ca. 0.3 mm) placed in a 5-mm-thick optical quartz cell and as thin (ca. 5 mg cm^{-2}) zeolite plates for FTIR measurements. NO adsorption (Merck, purity >99%, purified by

TABLE 1

Chemical Composition of Co–Ferrierites (Si/Al 8.4)

Zeolite	Co wt%	Co/Al
$CoNH_4$–FER	0.40	0.05
$CoNH_4$–FER	0.81	0.09
$CoNH_4$–FER	2.08	0.23
$CoNH_4$–FER	2.16	0.25
$CoNH_4$–FER	3.62	0.42
$CoNH_4$–FER	5.56	0.65
CoNaK–FER	1.01	0.12
CoNaK–FER	1.29	0.15
CoNaK–FER	1.52	0.18
CoNaK–FER	2.15	0.25
CoNaK–FER	2.47	0.28
CoNaK–FER	2.60	0.31

repeating freeze–pump–thaw cycles) took place at RT for 30 min on dehydrated (480°C in vacuum) Co–ferrierites at 0.7 and 45 Torr.

Co–ferrierites containing exchanged Co ions exclusively (see below) were chosen for EXAFS measurements. The samples for EXAFS measurements in the form of wafers were placed in a glass tube where they were treated under standard *in situ* conditions (480°C in vacuum) and sealed. The samples were transferred from the glass tube into the airtight EXAFS cell in a glove box under an inert atmosphere.

Spectroscopy

Optical spectroscopy. Diffuse reflectance (DR) UV–Vis–NIR spectra in the differential mode were measured using a Perkin–Elmer UV–Vis–NIR spectrometer (Lambda 19) equipped with a diffuse reflectance attachment; details of the spectrum recording and processing are given elsewhere (22, 23). The absorption intensity was calculated according to the Schuster–Kubelka–Munk function, $F(R_\infty)$. The values of the absorption coefficients for the α-, β-, and γ-type Co ions were determined before (23).

FTIR spectroscopy. Time-resolved IR spectra were monitored in the 4000- to 400-cm^{-1} range at RT on a Magna-IR System 550 FTIR (Nicolet) spectrometer using an MCT-B liquid-nitrogen-cooled detector and equipped with a heatable cell with NaCl windows connected to a vacuum system and a gas manifold. Details of the spectrum measurement and data processing are given in Ref. (27). The characteristic intensities of the B_M and B_{ML} bands in the region of the "transmission window," 900–950 cm^{-1}, for the perturbed antisymmetric T–O–T vibrations due to the presence of bare Co ions and Co–L complexes, respectively, were used to determine the concentration of locally perturbed T–O bonds adjacent to the bare Co ions and Co–L complexes. The assumption has been made that the extinction coefficients of the individual B_M and individual B_{ML} bands are equal.

EXAFS. EXAFS measurements were carried out at the European Synchrotron Radiation Facility ESRF (Grenoble, France) on the Swiss–Norwegian Beam Line (SNBL). Cobalt *K*-edge EXAFS spectra were recorded at liquid nitrogen temperature to decrease the Debye–Waller factors. Transmission and fluorescence measurements of the samples with higher and lower cobalt content, respectively, were carried out. Data were analyzed using the XAFS Data-Analysis Program XDAP, Version 2.2.2 (35, 36). Fourier transformation (FT) of the k^3-weighted EXAFS function (χ) was performed in the ranges 3.2–13.2 and 3.2–11.0 $Å^{-1}$ in the transmission and fluorescence modes, respectively. The Fourier filtered data were fitted in *R* space in the range 1.0–4.0 Å. The validity and goodness of fit were checked by fitting in *R* space as well as in *k* space using k^1-, k^2-, and k^3-weighted spectra. The FEFF7 program (37) was employed to calculate the spectra of reference compounds using XRD data for CoO, $CoSO_4$, and Co_2SiO_4 (38) as input parameters to obtain scattering amplitudes and phase shifts for Co–O and Co–Si/Al scattering pairs.

RESULTS

During the dehydration/deammination of Co–ferrierites, the samples changed their colour from pink to pale blue. The occurrence of only bare Co ions bound to framework oxygens in dehydrated Co–ferrierites was evidenced by the absence of water molecules in IR and NIR regions, the IR band of Co–OH groups at 3660–70 cm^{-1}, and their combination vibration bands at about 7300 cm^{-1} (not shown). The presence of bare Co(II) ions and their distribution among different cationic sites were preserved regardless of vacuum or oxygen heat treatment in the temperature range 460–510°C.

Co–Ferrierites Heat-Treated at 480°C under Vacuum

Figure 1 illustrates UV–Vis–NIR spectra of dehydrated parent H–FER and CoH–FER at different Co loadings. The bands characteristic for the *d–d* transitions of the Co(II) ions are in the ranges 5,000–8,000 and 14,000–22,000 cm^{-1}. An increase in the intensity of the spectrum from the UV up to the Vis region at high Co loadings can be ascribed to the appearance of the charge transfer (CT) bands, originating from non-cationic Co species formed at high Co loadings. It is hardly possible to estimate the amount of the Co oxide species in the zeolite from the spectral

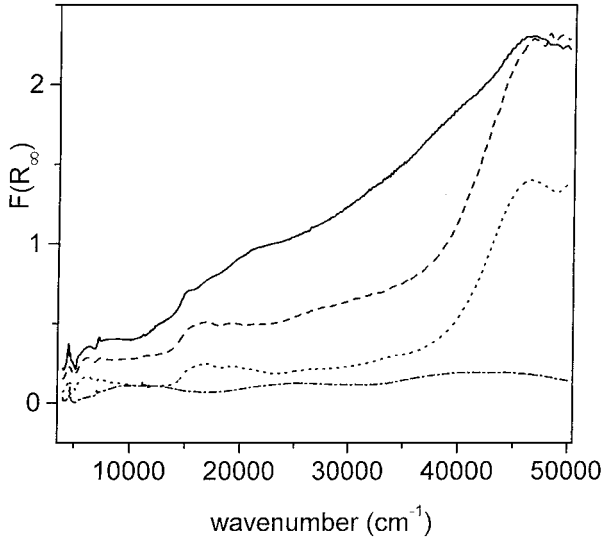

FIG. 1. DR UV–Vis–NIR spectra of H–FER and CoH–FER with different Co loadings. H–FER (·–·–·–·–); CoNaK–FER, Co/Al 0.28 (·····); CoH–FER, Co/Al 0.42 (–––––); CoH–FER, Co/Al 0.65 (——).

changes in the utraviolet region. The Vis spectrum of the highly loaded CoH–FER (Co/Al 0.65) did not show a clear band at 13,800 cm^{-1}, which was suggested by Fierro *et al.* (39) to reflect the presence of Co oxide species, although this "overexchanged" CoH–FER certainly contained some non-specified Co_xO_y species (see below).

Figure 2A shows Co(II) Vis spectra of the CoH–ferrierites dehydrated at 480°C, depending on the Co/Al ratio.

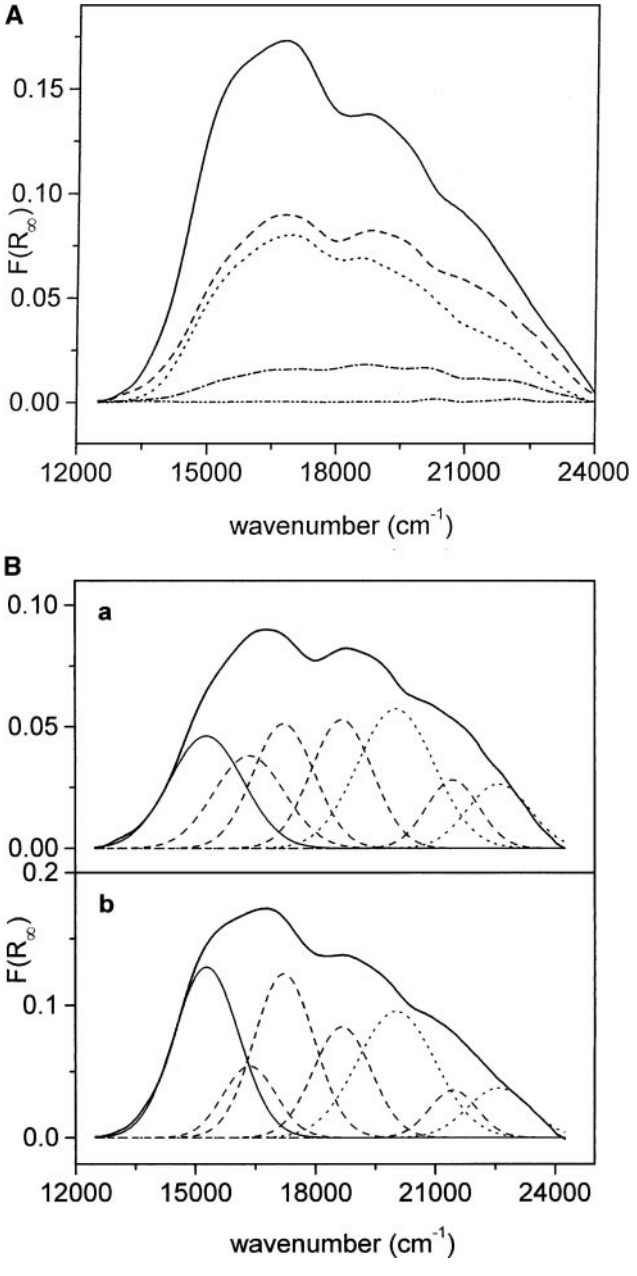

FIG. 2. DR vis spectra of CoH–FER with different Co loadings. (A) Co/Al: 0.42 (——), 0.25 (– – – –), 0.23 (· · · · · · ·), 0.09 (·–·–·–·–·–·), and 0.05 (·–· ·–· ·–). (B) Deconvolution of the DR vis spectra of CoH–FER Co/Al 0.42 (a) and 0.25 (b) into Gaussian bands of component α (——), β (– – – –), and γ (· · · · · · ·).

TABLE 2

Vis Spectra of the α-, β-, and γ-Type Co(II) Ions in Co–Ferrierites and the Corresponding Absorption Coefficients

Co(II) type	Wavenumbers (cm^{-1})				Absorption coefficient, 10^3 (cm)
α	15,000				1.3 ± 0.5
β	16,000	17,100	18,600	20,600	1.2 ± 0.3
γ	20,300	22,000			0.5 ± 0.2

It is clearly seen that with increasing Co loading the Vis spectra of the Co(II) ions increase in intensity and exhibit a different shape. This indicates a different distribution of the spectral components with different Co concentrations, and thus the occurrence of Co ions with different coordinations. Deconvolution of the Vis spectra to the individual bands for Co–ferrierites, as given elsewhere (23), is illustrated in Fig. 2B. It yielded three characteristic spectral components, α, β, and γ, reflecting the α-, β-, and γ-type Co ions (cf. Ref. (23)), which are given together with the corresponding absorption coefficients in Table 2.

FTIR spectra of dehydrated CoH–ferrierite samples at the same conditions (480°C) show a broad band (Fig. 3A) ascribed to the shifted antisymmetric vibrations of the T–O framework bonds induced by bonding of the Co(II) ions to the framework oxygens (27, 32). With increasing Co concentration, an increase in the intensity and changes in the shape of this broad band indicate the existence of several components. Deconvolution, given in Fig. 3B, yielded the individual B_M bands at 942, 918, and 905 cm^{-1}. This implies the existence of three different local perturbations of the framework T–O bonds induced by the bonding of three different Co sites to framework oxygen atoms. A linear correlation of the sum of the intensities of the bands at 942, 918, and 905 cm^{-1} obtained up to the Co/Al value of ca. 0.4 (Fig. 4), under the assumption that the extinction coefficients of the individual bands are the same, indicates that, up to this limit, the Co ions in ferrierite are mostly present as metal ions bound to framework oxygens at cationic sites. A deviation from the linearity at higher Co loadings (Co/Al > 0.4) suggests that, besides the exchanged cations, some Co ions occur in cobalt-oxide-like species, not affecting the T–O framework bonds.

The dependence of the relative concentrations of the α-, β-, and γ-type Co ions, as obtained from the intensity and absorption coefficients of the α, β, and γ Co(II) Vis spectral components (Table 2), and the intensity of the B_M bands at 942, 918, and 905 cm^{-1}, i.e., the relative concentration of the individual local framework perturbations induced by the Co ions, are given in Fig. 5. The good agreement in the trends of the relative concentrations of the α-, β-, and γ-type Co ions and those of the individual perturbed skeletal T–O–T bonds with Co loading strongly indicates a

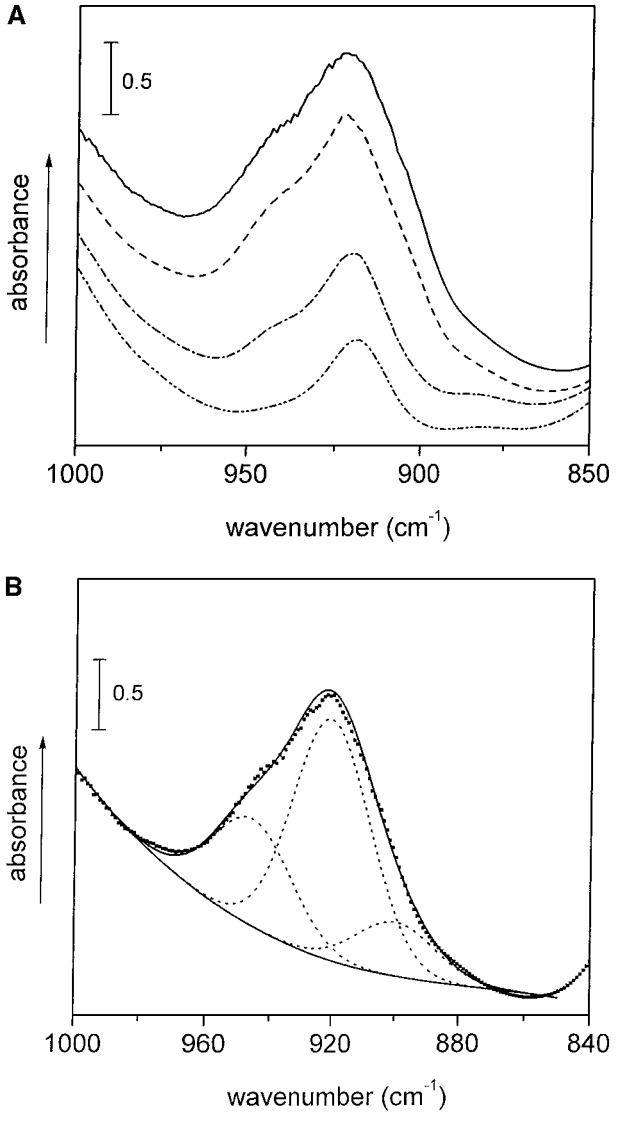

FIG. 3. FTIR spectra of skeletal vibrations of CoH–FER with different Co loadings. (A) Co/Al: 0.05 (·–· ·–· ·–), 0.09 (·–·–·–·–·–·), 0.25 (– – – – –), 0.42 (——). (B) Deconvolution of the FTIR spectra of CoH–FER, Co/Al 0.25 into Gaussian bands.

correspondence between the individual types of the Co ion siting at the α, β, and γ cationic sites and the individual local perturbations of the adjacent framework bonds reflected in the B_M bands at 942, 918, and 905 cm^{-1}.

EXAFS spectra were recorded on Co–ferrierites (see Table 3) in which one or two Co ion types prevailed. The concentration of the α-, β-, and γ-type Co ions was determined by quantitative analysis of the Co(II) Vis spectra. Experimental and Fourier-filtered spectra of CoNaK–ferrierite (1.7 wt%) and CoH–ferrierite (0.44 wt%) samples in reciprocal space are presented in Fig. 6. A general EXAFS model of the Co site common to all expected α, β, and γ centres was found to fit the data. The model consists of three coordination shells, where the first and

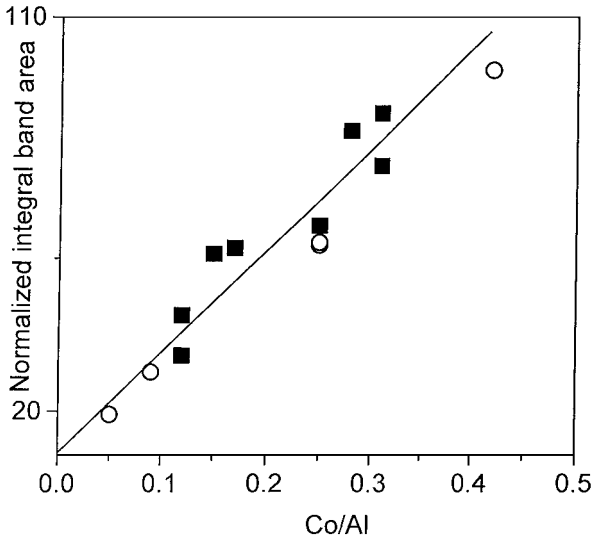

FIG. 4. Dependence of the integrated intensity of the sum of the skeletal B_M bands of CoH– (○) and CoNaK–FER (■) on Co loading.

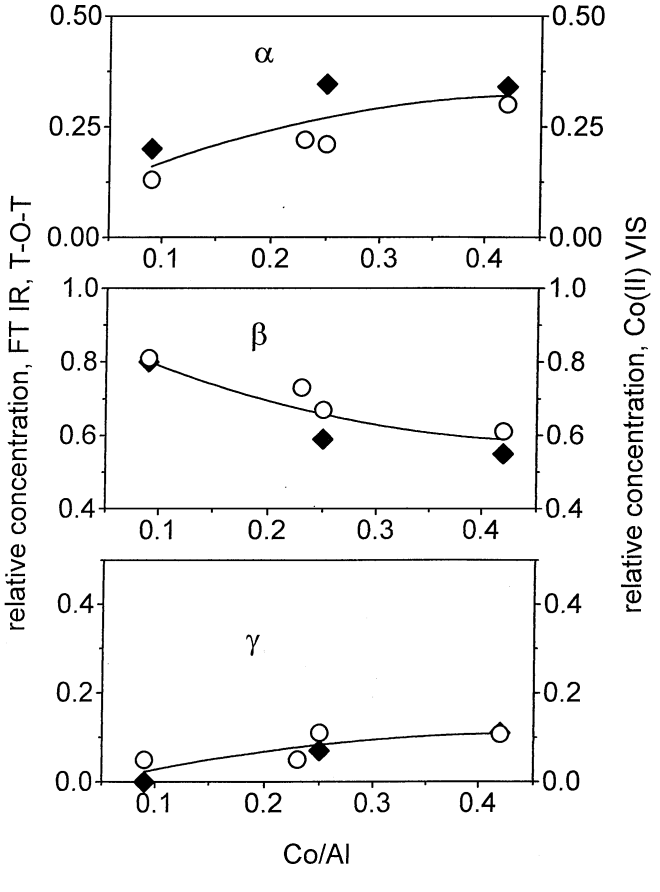

FIG. 5. Dependence of the relative concentrations of the α-, β-, and γ-type Co ions on Co loading. Concentrations obtained from Vis spectra (○) and IR skeletal B_M bands (◆); cobalt concentrations were calculated from the intensities of the Vis spectral components and corresponding absorption coefficients and from the intensities of the skeletal B_M bands under the assumption that the extinction coefficients are equal.

TABLE 3

EXAFS of Co–Ferrierites

Sample	CoNaK–FER						CoH–FER					
Co (wt%)/Co/Al	1.52/0.18						0.40/0.05					
$\alpha/\beta/\gamma$ (rel.%)	8/85/7						0/50/50					
	Transmission						Fluorescence					
	Three-shell fit			Four-shell fit			Three-shell fit			Four-shell fit		
Mode	R (Å)	C.N.	$\sigma^2 \times 10^{-3}$	R (Å)	C.N.	$\sigma^2 \times 10^{-3}$	R (Å)	C.N.	$\sigma^2 \times 10^{-3}$	R (Å)	C.N.	$\sigma^2 \times 10^{-3}$
Co–O(1)	1.99	3.5	3.5	1.99	3.0	2.4	1.99	3.4	2.9	1.93	3.2	8.7
Co–O(2)				2.09	1.7	8.1				2.00	1.3	2.9
Co–O(3)	2.85	2.3	1.1	2.85	2.9	2.3	2.91	3.1	1.3	2.89	2.7	1.5
Co–Si/Al	3.32	3.2	2.4	3.32	2.3	0.8	3.32	2.5	2.9	3.30	2.8	2.2

Note. R, interatomic distance; C.N., coordination number; σ, Debye–Waller factor.

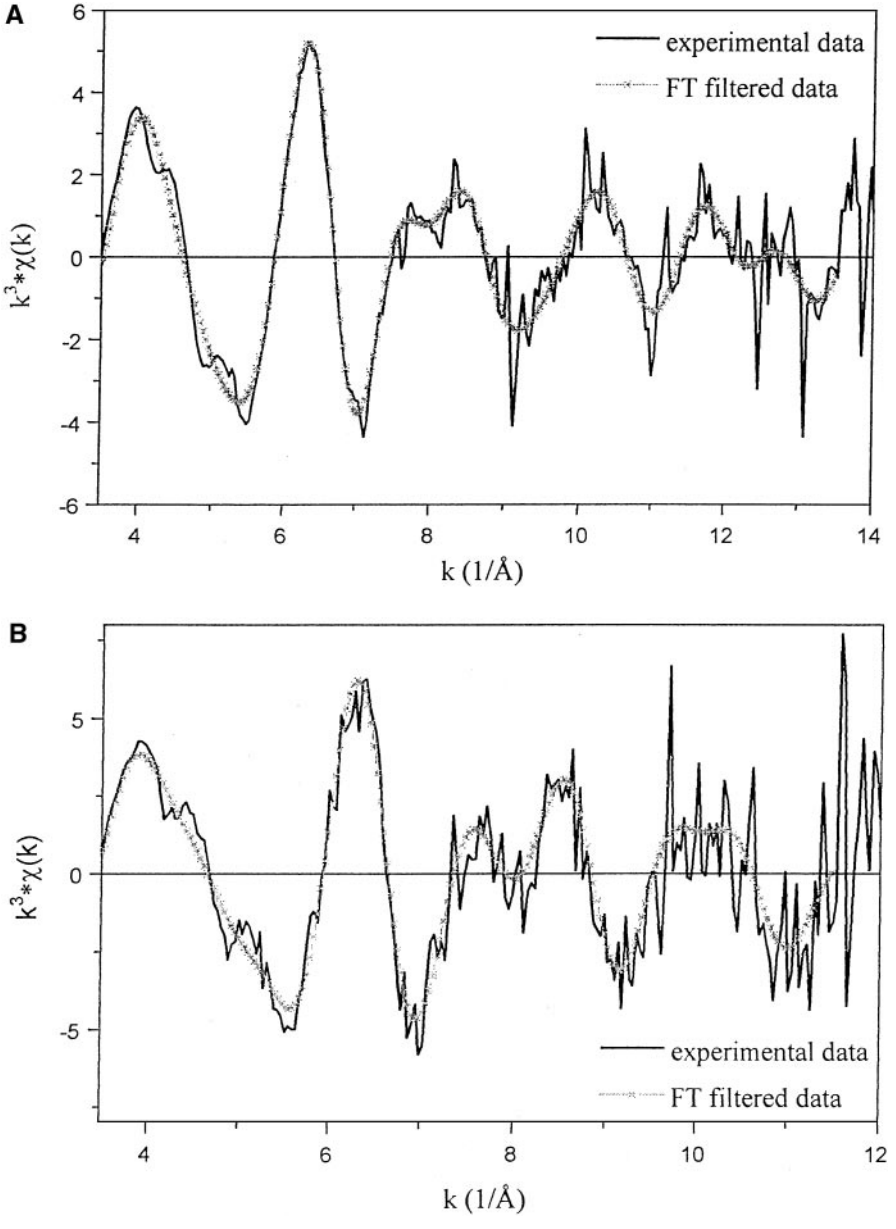

FIG. 6. Experimental and Fourier-filtered EXAFS χ functions of (A) CoNaK–FER (8/85/7) and (B) CoH–FER (0/50/50).

second shells correspond to the Co–O and the third shell to the Co–Si/Al back-scattering pairs (Fig. 7). Results of the fitting procedure (Table 3) provided a distance of 1.99 Å and a coordination number of 3.4–3.5 for the first oxygen shell in both Co-ferrierite samples. The distance of the second Co–O shell at 2.85 and 2.91 Å in CoNaK–ferrierite and CoH–ferrierite, respectively, seems to depend on the site population. In contrast, the distance of the third Co–Si/Al shell at 3.32 Å does not change.

An attempt to improve the fit was carried out by four-shell fitting, as shown in Fig. 8. The first Co–O shell of the three-shell fit is split into two very closely overlapping Co–O(1) and Co–O(2) shells in the four-shell fit (Table 3). Some changes in the Co–O(1) and (2) shell distances were observed with respect to the various distributions of the individual Co sites. The distances of the higher shells did not change in comparison with those of the three-shell fit.

Co–Ferrierites Calcined at 550°C on Air Followed by Hydration at RT and Evacuation at 480°C

The above Vis and FTIR spectra were monitored on CoH–FER samples dehydrated at 480°C in vacuum. After a higher temperature and prolonged calcination in air (550°C for 12 h), followed by hydration at room temperature and subsequent standard *in situ* dehydration at 480°C in vacuum, different relative intensities both of the α, β, and γ spectral components in the Vis spectra and of the individual skeletal B_M bands were observed (Figs. 9A and 9B, respectively). It is shown that the relative intensity of the spectral component α decreased in intensity (band at 15,000 cm^{-1}). Simultaneously, a significant increase in intensity of the B_M band at 918 cm^{-1} with a decrease in intensity of the B_M band at 942 cm^{-1} was observed. The intensity of the Vis spectral component γ (bands at 20,300 and 22,000 cm^{-1}) as well as the intensity of the B_M band at 905 cm^{-1} did not change compared to those for the standard Co–FER treatments (vacuum 480°C). The extent of the change in distribution of the Co ions due to the above treatment differed depending on the Co loading. The changes in the relative concentration of locally perturbed framework T–O bonds (B_M bands at 942, 918, and 905 cm^{-1}), i.e., those adjacent to the α-, β-, and γ-type Co ions, respectively, for CoH–FER with different Co loadings under zeolite treatment at 480 and 550°C, are depicted in Fig. 10. Substantial changes are found, particularly with CoH–FER at low Co concentrations, in contrast to those exhibiting close to the stoichiometric exchange degree, i.e., Co/Al $\approx$ 0.4.

NO Adsorption on Co–Ferrierites

After adsorption of NO on Co–FER, Co/Al 0.09, with the prevailing concentration of the Co ions (β type) inducing a skeletal B_M band at 918 cm^{-1}, the formation of cobalt mono- and dinitrosyls was found (Fig. 11). At low NO pressure, Co–NO complexes were detected by a single band at

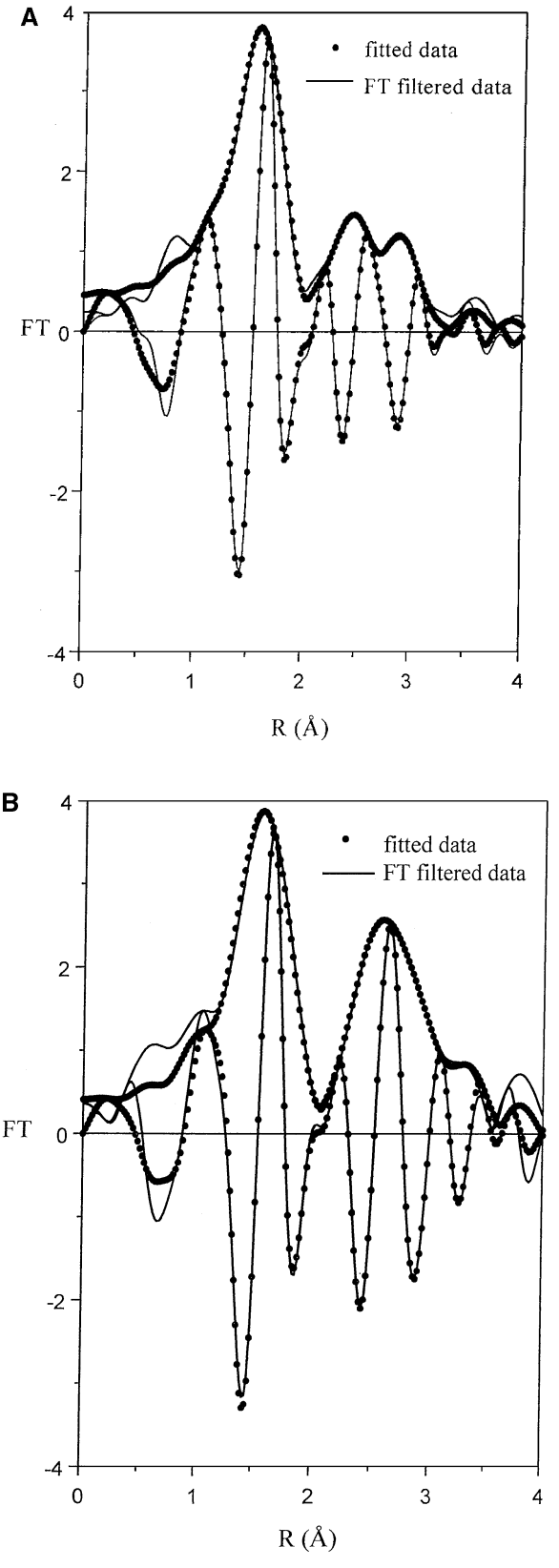

FIG. 7. Fourier transformation of filtered experimental data and fitted data of (A) CoNaK–FER (8/85/7) and (B) CoH–FER (0/50/50) using the three-shell fit.

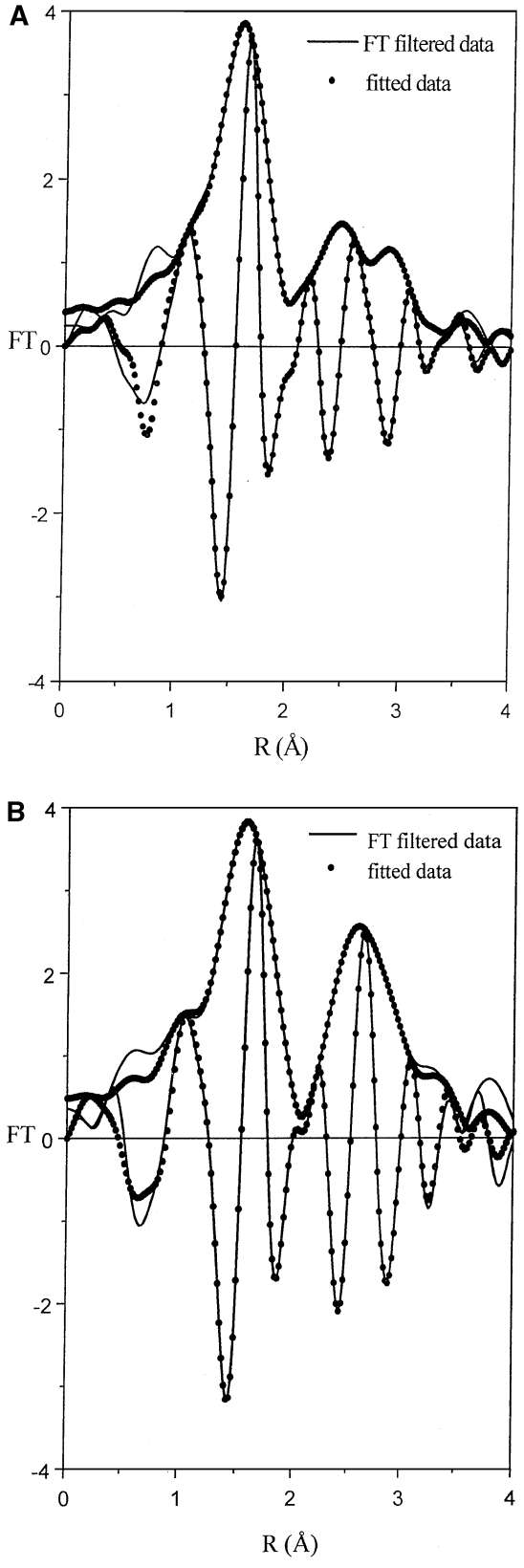

FIG. 8. Fourier transformation of filtered experimental data and fitted data of (A) CoNaK–FER (8/85/7) and (B) CoH–FER (0/50/50) using the four-shell fit.

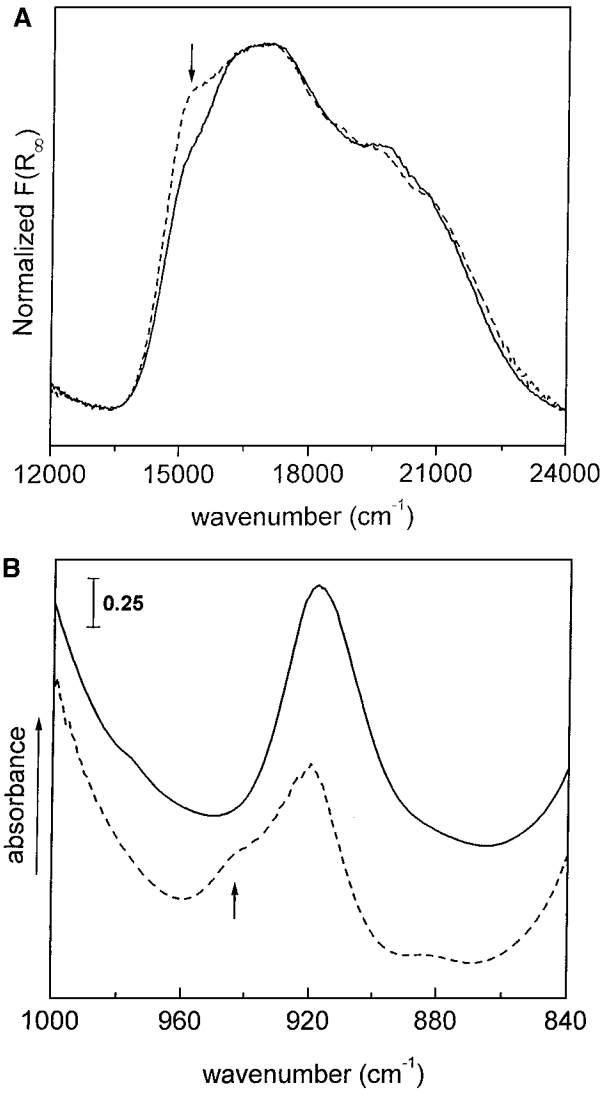

FIG. 9. Effect of treatment of CoH–FER on the DR Vis and FTIR spectra. Evacuation at 480°C (– – – – – –) and calcination at 550°C on air, followed by hydration at RT and evacuation at 480°C (——). (A) Normalized DR Vis spectra of Co–FER, Co/Al 0.25; (B) FTIR spectra of Co–FER, Co/Al 0.25.

1935 cm^{-1} in the region of NO vibration. The appearance of $Co(NO)_2$ at higher NO pressure was evidenced by intensive bands at 1898 and 1815 cm^{-1} with small shoulders at the lower frequency side of each band. In the region of skeletal vibrations, the formation of Co–NO as well as $Co(NO)_2$ complexes caused a shift in the originally perturbed antisymetric T–O vibration (induced by the bare Co ions, B_M band at 918 cm^{-1}) to the B_{ML} band at 933 cm^{-1}, that is, a "relaxation shift" of 15 cm^{-1}. No difference has been observed in the relaxation shift accompanying the formation of mono- or dinitrosyl complexes.

When adsorption of NO was carried out on Co–FER, Co/Al 0.25, containing roughly a comparable concentration of the α- and β-type Co ions, the framework bonds

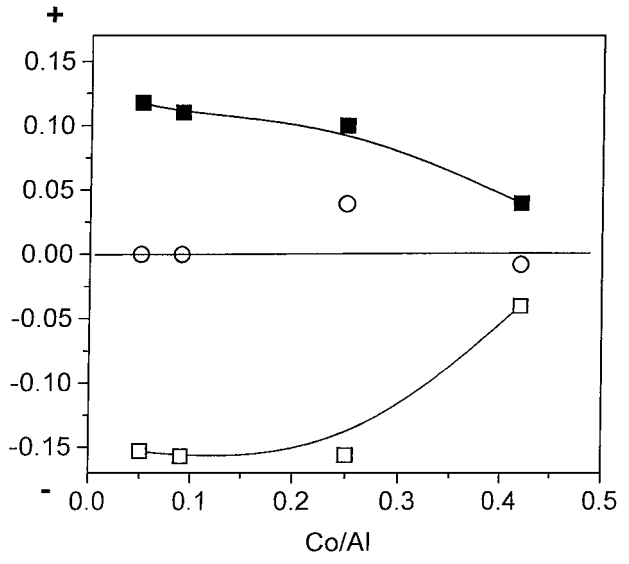

FIG. 10. Dependence of the changes in relative concentration of the α- (□), β- (■), and γ-type (○) Co ions in CoH–FER of different Co loadings, resulting from zeolite calcination at 550°C (followed by hydration and dehydration at 480°C), compared to the standard evacuation at 480°C, as obtained from the intensity of the IR spectra.

perturbed by bare Co ions, reflected in B_M bands at 942 and 918 cm^{-1}, were shifted after cobalt nitrosyls formation to 933 and 948 cm^{-1}, respectively. Thus, the relaxation shift of the T–O–T vibration connected with the adsorption of NO on the α-type Co ion attained a value of only

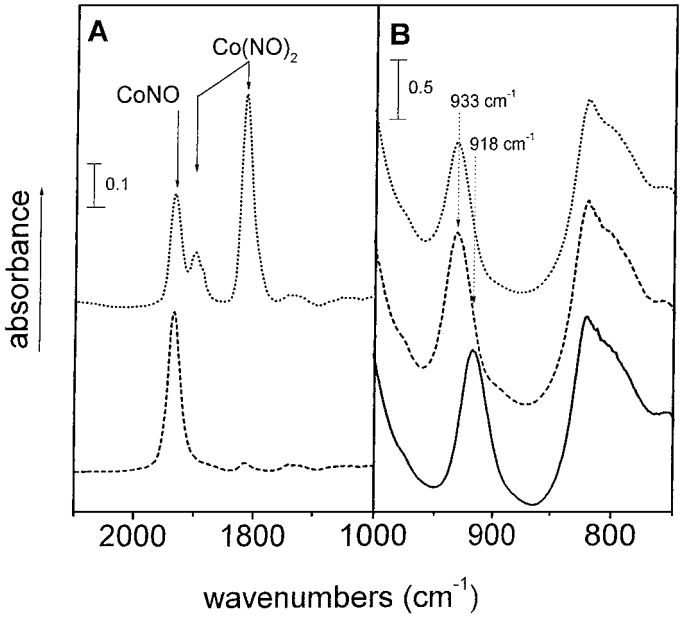

FIG. 11. FTIR spectra of CoH–FER, Co/Al 0.09 (——) evacuated at 480°C and after adsorption of NO (-----) at 0.7 Torr and (· · · · · ·) at 45 Torr.

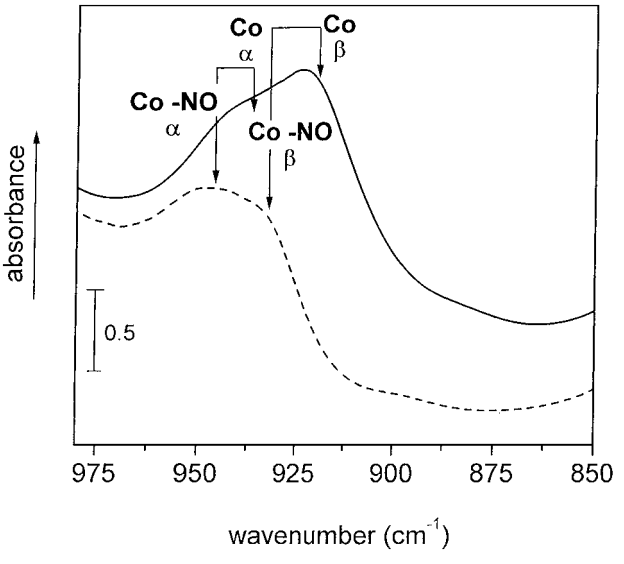

FIG. 12. FTIR spectra of CoH–FER, Co/Al 0.25 (——) evacuated at 480°C and (-----) after adsorption of 45 Torr NO.

6 cm^{-1}, roughly half of that found with the β-type Co ion (Fig. 12).

Quantitative analysis of the IR spectra of NO adsorption in the region of NO vibrations (1800–2200 cm^{-1}) of Co–ferrierites with wide Co concentration, and thus on the samples with different populations of the α, β, and γ sites by the Co ions, showed the preference of α-type Co ions for the formation of dinitrosyls compared to the β-type Co ions under the same conditions of NO adsorption (Fig. 13).

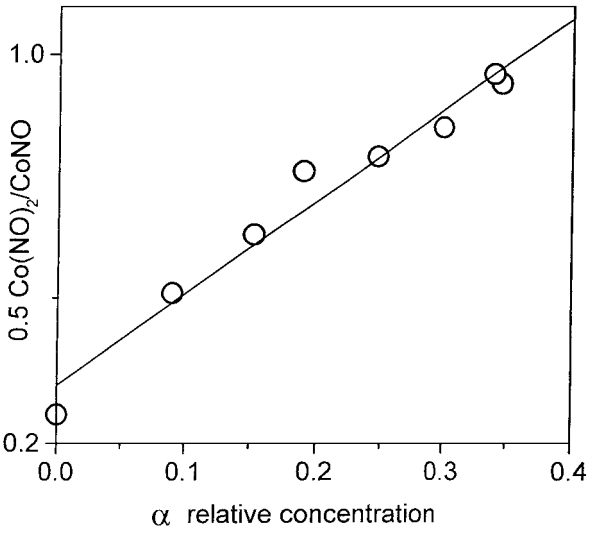

FIG. 13. Dependence of the ratio of dinitrosyl to mononitrosyl cobalt complexes on the relative concentration of the α-type Co ions in CoH–FER of different Co loadings.

DISCUSSION

Co Ions at Cationic Sites and in Undefined Co_xO_y Species

Incorporation of the Co(II) ions into cationic sites of ferrierite has been confirmed by a decrease in the intensity of the band at 3605 cm^{-1} and that at 7200 cm^{-1} of combination vibrations of the characteristic bridging OH groups (not shown in the figure). However, this finding did not disprove the theory that some of the Co(II) ions might also be present as noncationic undefined cobalt oxidic species, resulting from a partial hydrolysis of the Co ions during ion exchange. Presence of such Co oxidic species in ferrierite was suggested to be reflected in a band at 13,800 cm^{-1} (39). However, this band was not found, even with the overexchanged Co–ferrierite (Co/Al = 0.65). On the other hand, for such highly loaded Co–ferrierites and those with Co/Al > 0.4, the absorption intensity, ranging from the UV region to the Vis region, was substantially increased (see Fig. 1). This broad high intensity of absorption, likely reflecting charge-transfer effects, might indicate the presence of noncationic undefined Co oxidic species. This suggestion was supported by a quantitative analysis of the FTIR spectra of skeletal vibrations, showing a linear dependence (see Fig. 4) of the sum of the intensities of the B_M bands at 942, 918, and 905 cm^{-1} vs the Co concentration up to Co/Al $\approx$ 0.4. This indicates that all the exchanged Co ions provide characteristic perturbations of the T–O bonds forming the α-, β-, and γ-type cationic sites (see below). A deviation from this linearity at higher Co loadings indicates the existence of Co ions in undefined oxidic species. This conclusion on the highest attainable loading of the Co(II) ions at cationic sites (Co/Al = 0.4) in ferrierite with Si/Al = 8.4 is supported by the results of Lee *et al.* (40), who reported a linear correlation of the amount of NO adsorbed with the Co concentration up to Co/Al = 0.4 for Co–ZSM-5. Thus, up to a concentration of Co/Al $\approx$ 0.4 in ferrierite, it can be guaranteed that most of the Co ions are exchanged Co ions at cationic sites. Accordingly, with the aim to analyze the structure and properties of the exchanged Co ions in ferrierite, we carried out further studies with Co–ferrierites up to Co/Al = 0.4.

The α-, β-, and γ-Type Co Ions at Cationic Sites

Quantitative analysis of the intensity of the α, β, and γ Vis spectral components of the Co(II) ions of Co–ferrierites (Fig. 2) and the intensities of the B_M bands at 942, 918, and 905 cm^{-1} (Fig. 3) as the function of the Co concentration revealed a satisfactory match of the distribution of the α-, β-, and γ-type Co(II) ions and the concentration of the individual local T–O bonds perturbed to a different extent; B_M bands at 942, 918, and 905 cm^{-1} (Fig. 5). This finding evidences that the exchanged α-, β-, and γ-type Co(II) ions induce three characteristic perturbations of the local framework T–O bonds, i.e., perturbations of the framework T–O bonds at the individual cationic sites α, β, and γ. This conclusion is supported by the parallel changes in population of the α and β sites by the Co ions resulting from prolonged calcination at high temperature, as obtained from both the Co(II) Vis and the FTIR spectra in the range of the skeletal vibrations (cf. Figs. 9A and 9B).

The smallest perturbation of the framework bonds, the B_M band at 942 cm^{-1}, is connected with the α-type Co(II) ions. According to the previous Co(II) Vis study (23), these ions are suggested to be coordinated above the rectangle of framework oxygens of the six-member ring, formed by *connecting* five-member rings, in the main ten-member ring channel of ferrierite (see scheme in Ref. (23)). The β-type Co(II) ions, assumed to be coordinated to the deformed six-member ring in the ferrierite cavity, exhibit medium perturbation, corresponding to the B_M band at 918 cm^{-1}. The γ-type Co(II) ions, located in the boat-shaped site of ferrierite, likely in the most packed environment of framework oxygens of the three sites, possesses the largest perturbation of the adjacent T–O bonds, corresponding to the B_M band at 905 cm^{-1}. If we assume that the degree of perturbation of the T–O framework bonds, the deformation shift, corresponds to the strength of Co–O bonding, it follows that the strength of bonding of the Co ions to framework oxygens in cationic sites increases in the sequence $\alpha \ll \beta \leq \gamma$.

EXAFS results obtained from the three-shell fit of the spectra (Fig. 7, Table 3) show that the average Co site in ferrierite is represented by Co ions coordinated to four, eventually three, framework oxygen atoms at an average Co–O distance of 1.99 Å and to two or three framework oxygen atoms at a distance of 2.85–2.91 Å. This Co–O distance is, however, too long for direct coordination of the framework oxygen atoms to the Co ions. This shell is clearly attributed to the framework oxygens in the rings surrounding the Co cations. The last shell represented by Si or Al atoms at a distance of 3.30–3.34 Å is common to both Co–FER samples.

The Co–O distance of 1.99 Å, obtained from the three-shell fit, does not show any dependence on the population of the individual cationic sites by the Co ions. Therefore, only very small differences in the interatomic Co–O distances can be expected to characterise the α, β, and γ Co sites, which are too close to be determined by EXAFS. It can be expected that the results from the data analysis for CoNaK–FER, Co/Al 0.18 (Co β site 85%), represent the most frequently populated β site, which is almost exclusively populated in this sample. Therefore, the β site can be determined as a Co cation coordinated to four framework oxygen atoms at a distance of 1.99 Å and with two framework oxygen atoms of the six-member ring at a distance of 2.85 Å. Considering the same coordination number obtained for the mixture of β and γ sites (1 : 1, CoH-FER, Co/Al 0.05) and taking into account that the coordination

numbers obtained from EXAFS are usually slightly underestimated in the case of closely overlapping shells, it can be speculated that the Co cation in the γ site is coordinated to four framework oxygens at the same distance of 1.99 Å.

In agreement with the three-shell fit, the four-shell fit (Fig. 8) also shows that the Co ions are coordinated to four lattice oxygens. The ligand environment of the Co atom is formed by three oxygen atoms coordinated at shorter distances and one oxygen at a longer distance to the Co ion. It seems that small shifts in the distances observed in the four-shell fit are dependent on the site population. It can be speculated that the high concentration of the γ sites in the CoH–ferrierite sample shifts the distances to shorter values and thus it can be deduced that the average Co–O distances representing the site γ are shorter than the average distances, which belong to the β site. The Co–O distances for the α-type Co ions could not be estimated, as it is not possible to prepare a Co–ferrierite sample with a prevailing concentration of this type of Co ions.

These results are in good agreement with the reported mean values obtained from EXAFS of Co–zeolites (16, 17), our results for Co–ZSM-5 (43), the XRD Co–O bond distance data reported for A and Y zeolites (41, 42, 44), and theoretical calculations, which suggest that Co–O distances can vary between 1.8 and 2.1 Å (45). Generally, the results on the coordination of transition-metal ions such as Cu and Co in zeolite matrices indicate that these cations are distributed over the available sites to reach an optimum coordination with the framework, establishing a minimal potential energy (29, 45, 46). Theoretical calculations show that the presence of the metal ions induces a characteristic local distortion of the framework bonds, depending on the extent of ionic/covalent bonding of the cation to framework oxygens (29). Moreover, with the divalent Co ion the calculated distortions of the deformed six-member ring of ferrierite representing the β site clearly showed fourfold coordination of the cation to framework oxygen atoms at this site (29). The same cation coordination at the deformed six-member ring of ZSM-5, based on calculated perturbation of the framework bonds, was suggested by Datka and co-workers (47). For the Co(II) ions it has been suggested, using density functional theory (DFT), that they exhibit coordination numbers of 3, 4, or 5, depending on the Si/Al ratio (45).

The calculated Co–O distances obtained from the EXAFS data analysis of Co–ferrierites is typical for Co–O bonds, but they are shorter than the distances expected based on the rigid model of the ferrierite framework. This means that the Co ions deform the framework. This is exactly what we have clearly observed by the different perturbations of the T–O bonds adjacent to the individual Co ions and what was predicted by theoretical calculations (30, 45).

It can be concluded that a complementary set of spectroscopic methods used for the description of the Co ions at the cationic sites of ferrierite, i.e., Co(II) Vis, FTIR of skeletal vibrations, and EXAFS, provided a description of three characteristic Co ion types.

Changes in Population of the α and β Cationic Sites by the Co Ions in Dehydrated Co–Ferrierites after Zeolite High-Temperature Calcination and Hydration

The weakest bonding of the α-type Co ions and, in contrast, the strongest bonding and the shortest Co–O distance of the γ-type Co ions are also reflected in the changes of the distribution of the Co ions among the individual cationic sites after prolonged calcination (550°C) of Co–ferrierites. With Co–ferrierites, where some cationic sites were not occupied by Co ions or other cations, and the negative framework charge was balanced by protons, the relative population of the β sites by the Co ions was increased on account of the α-type Co ions. The extent of this effect was more pronounced with Co–ferrierites, where more free cationic sites were available (Figs. 9 and 10). In contrast, the concentration of the γ-type Co ions was not changed under high-temperature treatment, over the whole cobalt concentration range, even in the case where some cationic sites were unoccupied. The weakest bonding of the Co ions at the α sites and their transfer to the β sites under severe heat or hydrothermal treatment is similar to the behaviour of that type of Cu ions in ZSM-5, suggested to be balanced by a single AlO_2^- framework entity (48) and suggested by us to represent a similar α site located on the wall of the main channel of the MFI structure (11).

Coordinative Bonding of the Co Ions

The coordination and strength of bonding of the Co ions at the individual cationic sites were also reflected in their interaction with NO. At the same conditions of NO adsorption, the α-type Co ions exhibited a higher preference for the formation of dinitrosyls instead of Co–NO complexes, while the β-type Co ions formed more mononitrosyl complexes, as follows from the quantitative analysis of the IR spectra in the region of NO vibrations (cf. Figs. 11–13). Differences in the bonding of the α- and β-type Co ions were also reflected in the extent of perturbation of the adjacent framework bonds after NO adsorption. The value of this relaxation shift is a measure of the weakening of the cobalt–framework oxygen bonding due to ligation of NO molecule(s) to the Co ion. It is to be noted that the mononitrosyl as well as dinitrosyl Co ion complexes provided the same relaxation shift of the perturbed antisymmetric T–O vibration due to the coordination of individual bare Co ions. This implies that the strength of Co–O bonding was not significantly affected by the ligation of the second nitrosyl. However, the Co–O bonding of the individual Co ions was affected, to a different extent, by the formation of cobalt–nitrosyl complexes. The relaxation shift connected with the α-type Co ions was much smaller (6 cm^{-1}) than that

with the β-type Co ions (15 cm^{-1}); see Fig. 13. Therefore, the weakly bound Co ions at α sites were able to ligate NO without substantial weakening of the original Co–framework oxygen bond, in contrast to the Co ions in β sites, where bonding with framework oxygens was much more weakened after coordination of the NO molecule. It follows that the different types of exchanged Co ions in Co–ferrierites also exhibit different behaviour under interaction with NO with respect to both the composition of nitrosyl complexes and the weakening of the cobalt–framework oxygen bonds.

CONCLUSIONS

Three typical Co ion sites in ferrierite, previously suggested from the Co(II) Vis spectra and known ferrierite framework geometry, exhibit different perturbation of the hosted framework T–O bonds. The structure and behaviour of these sites, i.e., the polyoxo-anion–cobalt complexes, have been described by quantitative analysis of the Co(II) Vis spectra, FTIR spectra in the region of skeletal vibrations, and EXAFS measurements on Co–ferrierites with different Co loadings.

The α-type Co ions, exhibiting a Vis band at 15,000 cm^{-1} and a perturbed antisymmetric T–O vibration (B_M band) at 942 cm^{-1}, are coordinated to the rectangle of framework oxygens of the six-member ring, formed by connected two-folded five-member rings, on the wall of the main ten-member ring channel. The relatively open coordination sphere of these Co ions corresponds to their weak bonding to the framework oxygens and a high tendency to form dinitrosyl complexes under NO adsorption.

The β-type Co ions, with the Co(II) Vis spectral component consisting of bands at 16,000, 17,100, 18,700, and 20,600 cm^{-1} and with an antisymmetric T–O vibration at 918 cm^{-1}, are suggested to be coordinated to the deformed six-member ring of the ferrierite cavity. The β site has been shown to be the site most populated by the Co ions over the whole concentration range. Based on EXAFS results, four framework oxygen atoms are coordinated to the Co ion at a distance of 1.99 Å, while two additional framework oxygen atoms are at a substantially larger distance of 2.85 Å. The β-type Co ions exhibit medium strength bonding to framework oxygens, and compared to the α-type, the β-type Co ions have a substantially lower ability to form dinitrosyls.

The γ-type Co ions are reflected in the doublet of bands in the Vis spectral region (20,300 and 22,000 cm^{-1}) and in the perturbed antisymmetric T–O vibration at 905 cm^{-1}. These ions are located in a boat-shaped site of ferrierite. The γ-type Co ions, in agreement with the shortest Co–O distance and the highest extent of perturbation of framework T–O bonds, are the most strongly bound to framework oxygens.

The structure and character of bonding of the α-, β-, and γ-type Co ions are also reflected in their behaviour under high-temperature treatments.. The weakly bound α-type Co ions move to the β sites under severe thermal/hydrothermal treatment if the β sites are available in the zeolite. In contrast, the γ-type Co ions, exhibiting the strongest bonding to framework oxygens, did not change their siting, even under high-temperature treatment and hydrothermal conditions.

ACKNOWLEDGMENTS

The authors thank the Swiss–Norwegian Beamline staff for assistance during the EXAFS measurements at the ESRF. Authors from the J. Heyrovský Institute acknowledge financial support of the Academy of Sciences of the Czech Republic under Project S4040016 and of Air Products & Chemicals, Inc., Pennsylvania.

REFERENCES

1. Iwamoto, M., Yahiro, H., Tanda, K., Mizuno, N., and Mine, Y., *J. Phys. Chem.* **95**, 3727 (1991).
2. Li, Y., and Hall, W. K., *J. Catal.* **129**, 202 (1991).
3. Wichterlová, B., Dědeček, J., Sobalík, Z., Vondrová, A., and Klier, K., *J. Catal.* **169**, 194 (1997).
4. Iwamoto, M., and Yahiro, H., *Catal. Today* **22**, 5 (1994).
5. Feng, X., and Hall, W. K., *J. Catal.* **166**, 368 (1997).
6. Chen, H. Y., and Sachtler, W. H. H., *Catal. Lett.* **50**, 125 (1998).
7. Li, Y., and Armor, J. N., *J. Catal.* **150**, 376 (1994).
8. Li, Y., Slager, T. L., and Armor, J. N., *J. Catal.* **150**, 388 (1994).
9. Kikuchi, E., Ogura, M., Terasaki, I., and Goto, Y., *J. Catal.* **161**, 465 (1996).
10. Ohtsuka, H., Tabata, T., Okada, O., Sabatino, L. M. F., and Bellussi, G., *Catal. Lett.* **44**, 265 (1997).
11. Wichterlová, B., Dědeček, J., and Sobalík, Z., *in* "Proceedings 12th International Zeolite Conference, Baltimore, 1998" (M. M. J. Treacy, B. K. Marcus, M. E. Bisher, and J. B. Higgins, Eds.), p. 941. Materials Research Society, Warendale, PA, 1999.
12. Mortier, W. J., "Compilation of Extraframework Sites in Zeolites." Butterworth, London, 1982.
13. Attfield, M. P., Weigel, S. J., and Cheetham, A. K., *J. Catal.* **170**, 227 (1997).
14. Anpo, M., Matsuoka, M., Shioya, Y., Yamashita, H., Giamello, E., Morterra, C., Che, M., Patterson, H. H., Weber, S., Oullette, S., and Fox, M. A., *J. Phys. Chem.* **98**, 5744 (1994).
15. Lamberti, C., Bordiga, S., Salvalaggio, M., Spoto, G., Zecchina, A., Geobaldo, F., Vlaic, G., and Bellatreccia, M., *J. Phys. Chem. B* **101**, 344 (1997).
16. Tabata, T., Ohtsuka, H., Bellussi, G., and Sabatino, L. M. F., *in* "Proceedings 12th International Zeolite Conference, Baltimore, 1998" (M. M. J. Treacy, B. K. Marcus, M. E. Bisher, and J. B. Higgins, Eds.), p. 1169. Materials Research Society, Warendale, PA, 1999.
17. Park, Y. K., Goryashenko, S. S., Kim, D. S., and Park, S.-E., *in* "Proceedings 12th International Zeolite Conference, Baltimore, 1998" (M. M. J. Treacy, B. K. Marcus, M. E. Bisher, and J. B. Higgins, Eds.), p. 1157. Materials Research Society, Warendale, 1999.
18. Dědeček, J., and Wichterlová, B., *J. Phys. Chem.* **98**, 5721 (1994).
19. Dědeček, J., Sobalík, Z., Tvarůžková, Z., Kaucký, D., and Wichterlová, B., *J. Phys. Chem.* **99**, 16327 (1995).
20. Dědeček, J., and Wichterlová, B., *J. Phys. Chem. B* **101**, 10233 (1997).
21. Dědeček, J., and Wichterlová, B., *Chem. Phys. Phys. Chem.* **1**, 629 (1999).
22. Dědeček, J., and Wichterlová, B., *J. Phys. Chem. B* **103**, 1462 (1999).
23. Kaucký, D., Dědeček, J., and Wichterlová, B., *Microporous Mesoporous Mater.* **31**, 75 (1999).

24. Dědeček, J., Kaucký, D., and Wichterlová, B., *Microporous Mesoporous Mater.* **35–36**, 483 (2000).
25. Jacobs, W. P. J. H., van Wolput, J. H. M. C., and van Santen, R. A., *Zeolites* **13**, 170 (1993).
26. Sobalík, Z., Tvarůžková, Z., and Wichterlová, B., *Microporous Mesoporous Mater.* **25**, 225 (1998).
27. Sobalík, Z., Tvarůžková, Z., and Wichterlová, B., *J. Phys. Chem. B* **102**, 1077 (1998).
28. van Santen, R. A., and Vogel, D. L., *Adv. Solid-State Chem.* **1**, 151 (1989).
29. Šponer, J. E., Sobalík, Z., and Wichterlová, B., *in* "Proceedings, 12th International Congress on Catalysis, Granada, 2000" (A. Carma, F. V. Melo, S. Mendioros, and T. L. G. Eivro, Eds.), p. 1463. *Stud. Surf. Sci. Catal. B* **130**, Elsevier Amsterdam, 2000.
30. Lei, G. D., Adelman, B. J., Sárkány, J., and Sachtler, W. M. H., *Appl. Catal. B* **5**, 245 (1995).
31. Sun, T., Trudeau, M. L., and Ying, J. Y., *J. Phys. Chem.* **100**, 13662 (1996).
32. Sobalík, Z., Dědeček, J., Ikonnikov, I., and Wichterlová, B., *Microporous Mesoporous Mater.* **21**, 525 (1998).
33. Sobalík, Z., Belhekar, A. A., and Wichterlová, B., *Appl. Catal. A* **188**, 175 (1999).
34. Kaucký, D., Vondrová, A., Dědeček, J., and Wichterlová, B., *J. Catal.* **194**, 318 (2000).
35. van Zon, J. B. A. D., Koningsberger, D. C., van 't Blik, H. F. J., and Sayers, D. E., *Chem. Phys.* **82**, 5742 (1985).
36. Kirlin, P. S., van Zon, F. B. M., Koningsberger, D. C., and Gates, B. C., *J. Phys. Chem.* **94**, 8439 (1990).
37. Ankudinov, L., and Rehr, J. J., *Phys. Rev. B* **56**, R1712 (1997).
38. Sasaki, S., Fujino, K., and Takeuchi, Y., *Proc. Jpn. Acad.* **55**, 43 (1979). Rentzeperis, P. J., *Neues Jahrb. Mineral. Monatsh.* 226–233 (1958). Miyake, M., Nakamura, H., Kojima, H., and Marumo, F., *Am. Mineral.* **72**, 594 (1987).
39. Fierro, G., Eberhardt, M. A., Houalla, M., Hercules, D. M., and Hall, W. K., *J. Phys. Chem.* **100**, 8468 (1996).
40. Lee, C. W., Chong, D. J., Lee, Y. C., Chen, C. S., and Kevan, L., *Microporous Mater.* **12**, 21 (1997).
41. Riley, P. E., and Seff, K., *J. Chem. Soc. Chem. Commun.* 1287 (1972).
42. Gallezot, P., and Imelik, B., *J. Chim. Phy.* **71**, 155 (1974).
43. Drozdová, L., and Prins, R., unpublished results.
44. Riley, P. E., and Seff, K., *Inorg. Chem.* **13**, 1355 (1974).
45. Pierloot, K., Delabie, A., Ribbing, C., Verberckmoes, A. A., and Schoonheydt, R. A., *J. Phys. Chem. B* **102**, 10789 (1998).
46. Klier, K., Wichterlová, B., and Dědeček, J., *in* "Proceedings 12th International Zeolite Conference, Baltimore, 1998" (M. M. J. Treacy, B. K. Marcus, M. E. Bisher, and J. B. Higgins, Eds.), p. 40. Materials Research Society, Warendale, PA, 1999.
47. Broclawik, E., Datka, J., Gil, B., and Koryza, P., *Phys. Chem. Chem. Phys.* **2**, 401 (2000).
48. Kucherov, A. V., Slovetskaya, K. I., Goryashenko, S. S., Aleskin, E. G., and Slinkin, A. A., *Microporous Mater.* **7**, 27 (1996).